FISEVIER

Contents lists available at ScienceDirect

Computational Materials Science

journal homepage: www.elsevier.com/locate/commatsci



Misfit strain induced phase transformation at a basal/prismatic twin boundary in deformation of magnesium



Peng Chen^{a,b}, Fangxi Wang^{a,b}, Bin Li^{a,b,*}

- ^a Department of Chemical and Materials Engineering, University of Nevada, Reno, USA
- ^b Nevada Institute for Sustainability, University of Nevada, Reno, USA

ARTICLE INFO

Keywords: Magnesium Phase transformation Twinning

ABSTRACT

Phase transformation from hexagonal close-packed (HCP) to face-centered cubic (FCC) does not occur in plastic deformation of pure magnesium. In this work, a reversible HCP \rightarrow FCC phase transformation was observed at basal/prismatic twin boundary (TB) of $\{1\ 0\ \bar{1}\ 2\}$ twinning mode, in atomistic simulations of TB migration in pure magnesium. The FCC phase was induced by a local misfit strain between the parent and the twin. When an FCC phase was formed at the basal/prismatic TB, the TB migration was temporarily hindered. As the strain increased, the FCC transformed to the HCP twin by atomic shuffling. The orientation relationship between the FCC and the HCP parent satisfies $(11\ 1)_{FCC} \|(1\ 0\ \bar{1}\ 0)_{HCP}$. During transformation, a double-layered prismatic plane was transformed into a $(11\ 1)_{FCC}$ close-packed plane of the FCC by shear and shuffle. The energy barriers for the reversible phase transformation was calculated.

1. Introduction

Magnesium (Mg) and its alloys have potential applications in automotive and aerospace industries due to their low density and high specific strength. Because of their low-symmetry hexagonal close-packed (HCP) crystal structures, the plastic deformation mechanisms are very complicated and not fully understood. Generally, during plastic deformation, dislocation slip, i.e. basal [1,2], prismatic [2,3] and pyramidal [4–8] dislocations can be activated, as well as deformation twinning which plays an important role in the mechanical properties of Mg and other HCP metals. The most common twinning mode in Mg is $\{1\,0\,\bar{1}\,2\}\langle 1\,0\,\bar{1}\,\bar{1}\rangle$ extension twinning and has been reported extensively in the literature [9–11].

 $\{10\,\bar{1}\,2\}\langle10\,\bar{1}\,\bar{1}\rangle$ twinning mode presents many interesting properties that starkly contrast classical twinning behavior. In classical twinning, a homogeneous simple shear on the first invariant plane, aka the K_1 plane or twinning plane, is the key element that reorients the parent lattice to the twin lattice. Such a simple shear is accomplished by twinning dislocations which can only glide on the twinning plane [10]. This crystallographic relationship requires that the twin boundary (TB) be coherent and the boundary plane coincide with the twinning plane [12,13]. Extensive experimental observations of twinning in face-centered-cubic (FCC), body-centered-cubic (BCC) metals and other twinning modes in HCP materials validate the classical twinning theory except for $\{10\,\bar{1}\,2\}\langle10\,\bar{1}\,\bar{1}\rangle$ mode. This twinning mode, irrespective of

materials, departs from the classical definition of twinning [14–18]. Partridge [19] first observed that {1012} TBs can evolve into extremely incoherent structures using optical microscopy. Serra et al. [20,21] found that in atomistic simulations, TBs do not migrate on the {1012} twinning plane, unlike other twinning mode in HCP, and they proposed that TB migration is controlled by "disconnections" rather than "zonal twinning dislocations". However, as pointed out recently by Li and Zhang [14,22], the major deficiency of the disconnection model is that lattice correspondence [10] in deformation twinning is neglected. When lattice correspondence was analyzed [14,23], the twinning mechanism in the disconnection model was found exactly the same as the Li-Ma shuffling model [24] in which the twinning process is achieved via "parent basal to twin prismatic" and "parent prismatic to twin basal" lattice transformation solely mediated by atomic shuffling.

Recently, another anomalous behavior in $\{10\,\bar{1}\,2\}$ twinning was reported, which showed that an FCC phase appeared at TBs [25–27]. In atomistic simulations of deformation of Mg and Ti, Zhang et al. [25] and Ren et al. [26] showed that a wedge-shaped FCC phase nucleates at a $\{10\,\bar{1}\,2\}$ TB and separates the twin from the parent. However, no detailed analysis was provided in these works. More recently, Hirth et al. [27] reported that atomic layers of FCC structure were produced at a $\{10\,\bar{1}\,2\}$ TB and eventually sandwiched by the parent and $\{10\,\bar{1}\,2\}$ twin. They proposed that the FCC phase was generated by "disconnections pairs" possibly due to the low free energy difference between the HCP and FCC. Several questions arise: why the FCC phase can only be

^{*}Corresponding author at: Department of Chemical and Materials Engineering, University of Nevada, Reno, USA. *E-mail address*: binl@unr.edu (B. Li).

formed at $\{10\bar{1}2\}$ TBs but not in other twinning modes? What is the formation mechanism of an FCC phase at $\{10\bar{1}2\}$ TBs?

The purpose of this work is to investigate and resolve the formation mechanism of an FCC phase at basal/prismatic $\{1\,0\,\bar{1}\,2\}$ TBs, by using atomistic simulations. The results obtained further elucidate the non-classical nature of $\{1\,0\,\bar{1}\,2\}\langle 1\,0\,\bar{1}\,\bar{1}\rangle$ twinning mode which is the most important mode in HCP metals.

2. Simulation method

The molecular dynamic (MD) simulations were performed using the Large-scale Atomic/Molecular Massively Parallel Simulator (LAMMPS). The embedded atom method (EAM) potential [28,29] for Mg-Al binary system was used in this work. This EAM potential was well developed by Liu et al. [30] and has been widely used in numerous atomistic simulations of deformation mechanisms in Mg [31,4,25,32]. Simulations of tension and compression were performed. The simulation systems were fully relaxed before an external strain was applied. Details of the systemic configurations in the simulations are presented below. The strain was generated by moving atoms on one of the end surfaces at a constant displacement rate of 0.01 nm per ps. Free surfaces were applied to all three dimensions. The data of all simulations was collected every 0.5 ps. The visualization tool Ovito [33] was used to analyze the simulation results. Common neighbor analysis (CNA) [34] was used to distinguish different crystal structures and lattice defects.

To examine the energy difference between the HCP and FCC phases, quantum mechanics calculations based on the density-functional theory (DFT) was performed. The Vienna Ab-initio Simulation Package (VASP) [35–37] was used for our calculations. The Projector Augmented Wave (PAW) [38,39] and the Generalized Gradient Approximation of Perdew-Burke-Ernzerhof (GGA-PBE) [40] were applied. A Monkhorst-pack $13\times13\times13$ mesh was used. The total energy cutoff value of 600 eV was chosen, and the electronic self-consistent field was set at $10^{-6}\,\mathrm{eV}/$ Å in our simulation.

3. Results

3.1. $HCP \rightarrow FCC \rightarrow HCP$ transformations under tension and compression

The initial configuration for simulating the migration of a $\{10\,\bar{1}\,2\}$ twin boundary (TB) when a compressive load was applied perpendicular to the c-axis of the parent is shown in Fig. 1, which presents a 2D cross-sectional view. The dimension of the simulation system is $18\times25\times18\,\mathrm{nm}^3$, containing 350,479 atoms. The stain rate is $5.5\times10^{10}/\mathrm{s}$. The two crystals have a misorientation of $90^\circ\langle1\,\bar{2}\,10\rangle$, i.e. the initial TB is a basal/prismatic (B/P) interface which is denoted by yellow dashed line. The left crystal is the twin, and the right crystal is the parent. The compressive strain was applied along the $[10\,\bar{1}\,0]$ of the

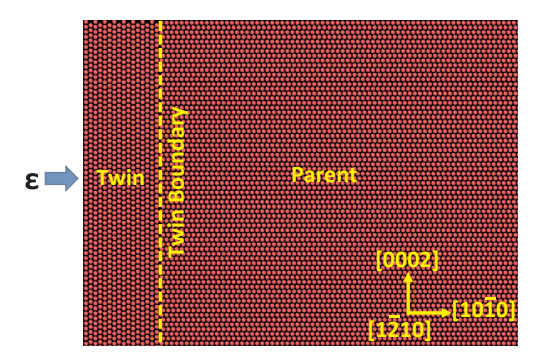


Fig. 1. Initial configuration for simulating twin boundary (TB) migration in magnesium under compressive loading in perpendicular to the c-axis of the parent. The two crystals have a misorientation of 90° $\langle 1\bar{2}10 \rangle$. A compressive strain was applied along the $[10\bar{1}0]$ direction of the parent.

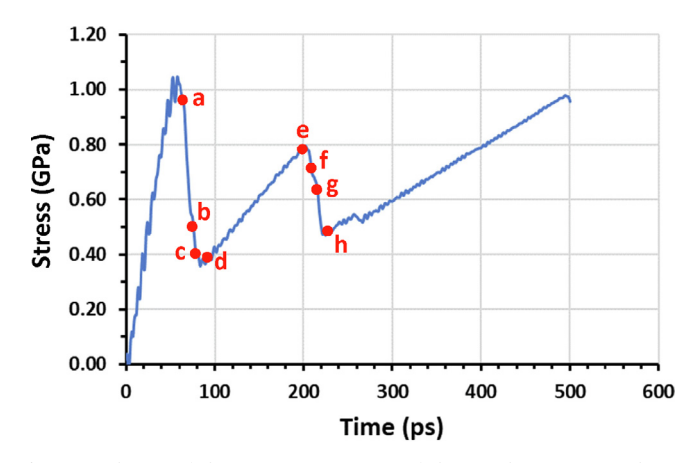


Fig. 2. Evolution of the compressive stress of the simulation system during deformation. The stress increases as the deformation proceeds. When the TB starts migrating, the stress drops rapidly. When the migration of the TB is paused, the stress increases again, until the stress is high enough to resume the migration of TB, then the stress drops again. When the migration of the TB is paused again, the stress increases again correspondingly. The red dots correspond to the snapshots displayed in Fig. 3.

parent. This loading condition favors $\{1\,0\,\bar{1}\,2\}$ extension twinning.

Fig. 2 shows the stress evolution of the simulation system during compression. The red dots correspond to the snapshots of the atomic structure displayed in Fig. 3 which shows the migration of the TB in time sequence. Initially, the system was elastically deformed, and the stress increases almost linearly. A sudden drop in stress occurs and this corresponds to the beginning of TB migration. The stress increases again followed by another drop. This serrated nature in the stress evolution is closely related to the structural change on the TB (see below).

In the CNA analysis, the HCP and FCC structure are colored in red and green, respectively, whereas other atoms on the free surfaces or the TB are colored in white and blue. After the compressive strain was increased to a critical value, the initial B/P TB started migrating toward the parent. It can be seen that the TB bulges out toward the parent and overall the TB becomes very incoherent, which is composed of incoherent B/P interfaces (Fig. 3a). As soon as the TB migrates, the stress decreases (see Fig. 2). The incoherent nature of the TB is consistent with experimental observations reported in the literature [14,18]. As the strain increases, the whole TB migrates and mostly evolves into B/P interfaces (Fig. 3b). Interestingly, a layer of green atoms emerge along the B/P segment, indicating the nucleation of an FCC phase on the TB. The green zone grows thicker as more layers of green atoms appear on the TB (Fig. 3c). As the new phase is forming on the B/P TB, the TB migration slows down. Eventually, the new phase grows and reaches the top surface. Meanwhile, another FCC phase appears near the bottom surface (Fig. 3d). The FCC phases create two wedge-shaped zones along the TB, and the TB migration comes to a halt. This corresponds to an increase in the stress to resume the TB migration (Fig. 2). As the strain builds up, the TB migrates again, initiating at the tips of the two wedgeshaped FCC phases (Fig. 3e). The FCC phases gradually disappear by transforming to the twin as the TB bulges toward the parent (Fig. 3f). Eventually the FCC phases are totally transformed to the twin (Fig. 3g). As the TB is migrating and the FCC phases are transforming to the twin, a relaxation occurs to the system and this corresponds to the second stress drop in Fig. 2. At the end of the second relaxation, new FCC phases form again on the B/P interface and the TB migration pauses again (Fig. 3f).

To quantitatively evaluate the energy barrier for the $HCP_{parent} \to FCC \to HCP_{lwin}$ phase transformation on the TB, we computed the potential energy of three layers of the FCC structure which contains 263 atoms and plotted the evolution of the energy during

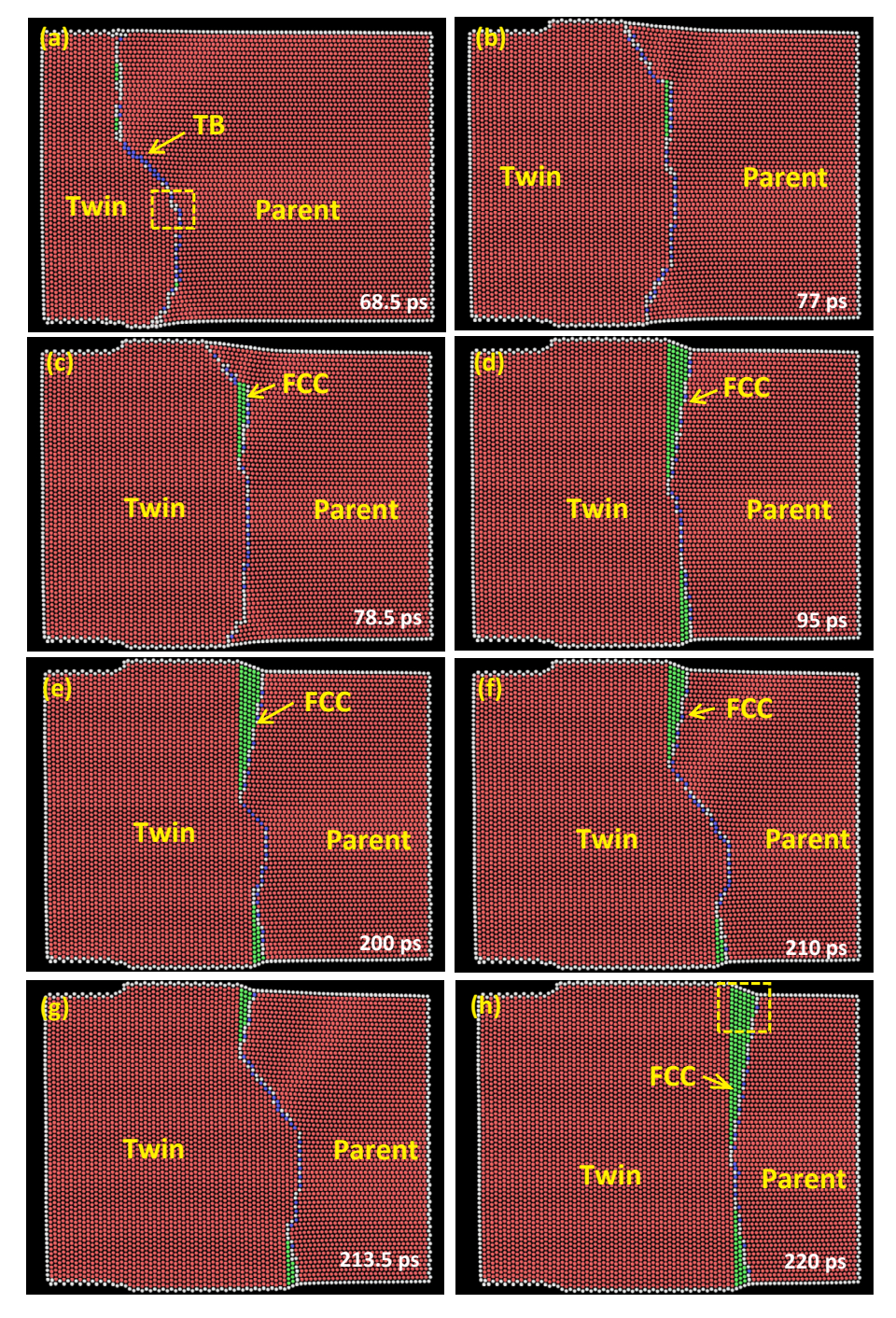


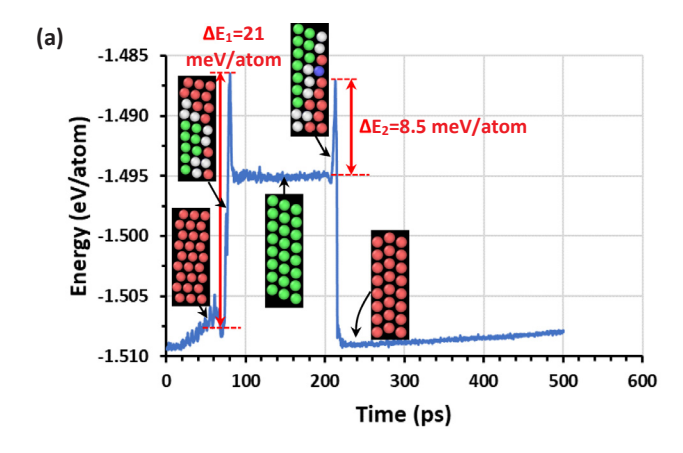
Fig. 3. Migration of twin boundary (TB) in time sequence. (a) When the compressive strain reaches a critical value, the TB starts migrating. The boxed region was selected for computing the energy evolution. Note the TB remains very incoherent. (b) An FCC structure (atoms in green) appears at the TB. (c) The FCC phase grows. (d) The FCC phase grows along the TB and intersects with free surfaces. As a result, the TB migration is paused. (e) As the strain builds up, the TB resumes migrating, as the FCC phase is receding. (f) The TB further bulges toward the parent as the FCC phase is disappearing. (g) The TB migration consumes the FCC phase. (h) New FCC phase forms again and the TB migration is paused again.

deformation. The result is shown in Fig. 4a. Under the external strain, the energy gradually increases due to the elastic stretching in atomic bonds. As the deformation further proceeds, at $\sim\!77~\rm ps$, a sharp increase in the potential energy occurs, and this corresponds to the nucleation of the FCC structure at the TB. After the selected atoms are completely transformed into the FCC structure, the energy plummets. Thus, the energy barrier of the transformation from the HCP parent to the FCC structure is $\sim\!21~\rm meV/atom$. As the deformation continues, the FCC structure stays stable at the energy level of about $-1.495~\rm eV/atom$ from 100 ps to 210 ps. As the external strain builds up, the TB starts migrating again by transforming the FCC phase to the HCP twin. An energy peak appears at $\sim\!212~\rm ps$, corresponding to the transformation from the FCC to the HCP twin. Thus, the energy barrier of this reverse transformation is about $8.5~\rm eV/atom$.

Similarly, we can evaluate the energy barrier of twin growth by

plotting the energy evolution of the selected box which contains 168 atoms (see Fig. 3a). The result is shown in Fig. 4b. It can be seen that when the TB passes the box, the energy is increased sharply. After this region is totally twinned, the energy plummets. Thus, the energy barrier for the twin growth is about 11.9 eV/atom, which is a reasonable value compared to the energy barrier for homogeneous $\{1\,0\,\bar{1}\,2\}$ twin nucleation (~27 meV/atom) for Mg [41]. For clarity, in these energy plots, local structures are also provided at different energy states.

To determine the orientation relationship (OR) between the FCC structure and HCP lattice, the boxed region in Fig. 3h was selected and analyzed in Fig. 5. The unit cells of the parent, twin and FCC structure are indicated by dashed rectangles. The basal plane of the HCP and the $\{1\,1\,1\}$ plane of the FCC are marked out. The OR can be determined as $(0\,0\,0\,2)_T \|(1\,1\,1)_{FCC}\|(1\,0\,\bar{1}\,0)_P$. For HCP \rightarrow FCC transformation in HCP metals, two types of orientation relationships were reported in the



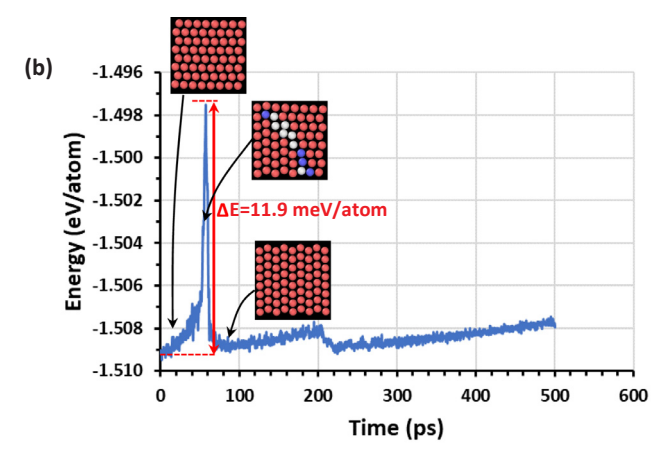


Fig. 4. (a) Energy evolution during phase transformation at the twin boundary (TB). The energy barrier for transformation from hcp to fcc is $\sim 21 \, \text{meV/atom}$, and the energy barrier for the reverse transformation is $\sim 8.5 \, \text{meV/atom}$. (b) The energy barrier for twin growth is $\sim 11.9 \, \text{meV/atom}$.

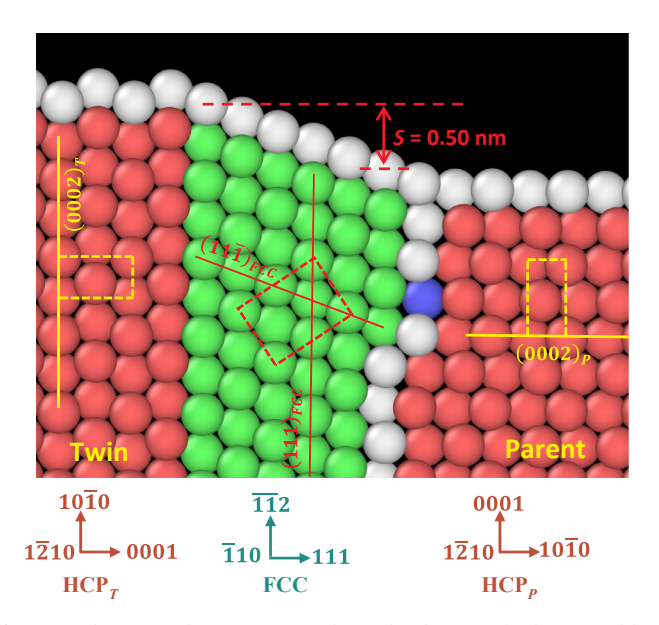


Fig. 5. To determine the orientation relationship between fcc lattice and hcp lattice, the boxed region in Fig. 3h was selected and analyzed. The unit cells of the parent, twin and fcc structure are indicated by dashed lines. The orientation relationship can be described as $(0\,0\,0\,2)_T \|(1\,1\,1)_{FCC}\|(1\,0\,\bar{1}\,0)_P$. The shear displacement for 5 layers of $(1\,1\,1)$ plane is 0.50 nm. Thus, the magnitude of the shear on each layer is 0.10 nm, and this corresponds to half a Burgers vector of a Shockley partial.

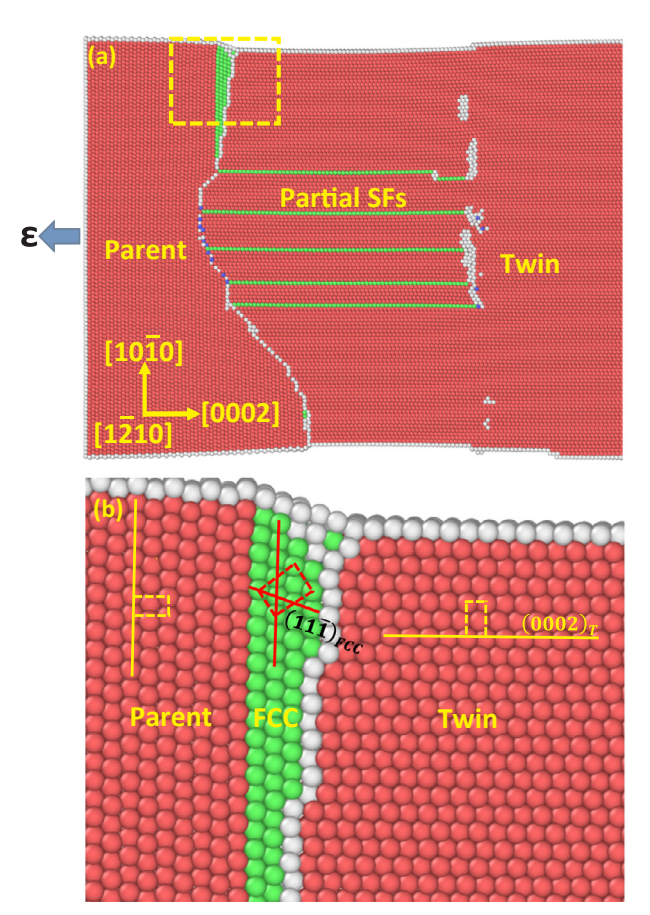


Fig. 6. (a) An FCC phase also forms when a tensile load is applied along *c*-axis of the parent. (b) The boxed region in (a) is magnified. The orientation relationship between the FCC, parent and twin is $(0\,0\,0\,2)_F \|(1\,1\,1)_{FCC}\|(1\,0\,1\,0)_T$.

literature: $\{0002\}_P \quad ||\{111\}_{FCC}, \quad [11\bar{2}0]_P ||[110]_{FCC} \quad [42–44], \text{ and } \{10\bar{1}0\}_P ||\{1\bar{1}0\}_{FCC}, [0001]_P ||[001]_{FCC} \quad [26,45–48]. \text{ Thus, the OR in this work, i.e. } (111)_{FCC} ||(10\bar{1}0)_P, \text{ is different from the previously reported ORs. Additionally, a large misfit } (\sim 0.54 \, \text{nm}) \text{ in the vertical direction between the parent and twin can be observed. It can also be seen that a shear deformation occurred in the FCC phase, and the shear displacement over 5 layers of the close-packed planes is <math>\sim 0.50 \, \text{nm}$, thus the shear displacement on each plane is $\sim 0.10 \, \text{nm}$.

The HCP \rightarrow FCC transformation occurred during compression perpendicular to the c-axis of the parent. To investigate if similar phenomenon also occurs under tension along the c-axis of the parent, we performed simulation by reversing the compressive load to a tensile load. The dimension of this simulation system is $20 \times 40 \times 30 \, \mathrm{nm}^3$, containing 1,035,000 atoms. The stain rate is $5.0 \times 10^{10}/\mathrm{s}$. The results are shown in Fig. 6. Indeed, during TB migration, an FCC phase appears along the B/P TB (enclosed in the dashed box near the top surface). Meanwhile, several partial stacking faults (SFs) are formed inside the twin, with one end attached to the migrating TB. In the CNA, SFs created by partial dislocations should appear to be two layer of green atoms. In contrast, the SFs in Fig. 6a appear to be one layer of green atoms and they are partial SFs first defined by Song and Gray [15,16].

Fig. 6b shows a magnified view of the boxed region in Fig. 6a. It can be seen that the structure of the FCC phase and the OR between the HCP parent, FCC and HCP twin are very similar to that in compression. The OR satisfies $(0\,0\,0\,2)_P \,\|\,(1\,1\,1)_{FCC} \,\|\,(1\,0\,\bar{1}\,0)_T$. The difference is that in tension, the FCC structure is transformed from the twin, which is also accomplished by the transformation of a double layered prismatic plane of the twin to a single layered $(1\,1\,1)_{FCC}$ plane of the FCC, if compared to Fig. 5. A shear is also involved as it can be seen on the top surface.

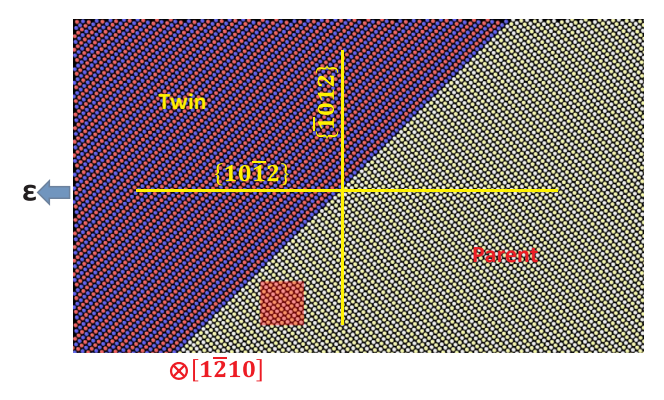


Fig. 7. The initial configuration for simulating the phase transformation at a twin boundary (TB) when the TB is oriented about 45° with the loading direction. Two crystals were bonded together and had a misorientation of 90° with a zone axis of $[1\bar{2}10]$. The basal planes of the two crystals were colored alternately to show the ...ABABAB... stacking sequence. A tensile strain was applied along the horizontal direction, i.e. making 45° with basal planes of the parent and twin. Atoms inside the red box were selected for computing the energy barrier of transformation from HCP to FCC structure.

3.2. $HCP \rightarrow FCC$ transformation with a high resolved shear stress on B/P TR

In the simulations of tension along the c-axis and compression perpendicular to the c-axis of the parent crystal, $\{10\bar{1}2\}$ twinning is strongly favored. In both cases, an FCC phase appears on the B/P TB during TB migration. To further understand how FCC phase is formed during twinning, we investigated a special configuration in which $\{10\bar{1}2\}$ twinning is not favored; instead, the basal/prismatic interface, i.e. an incoherent {1012} TB, is oriented such that the TB has a maximum Schmid factor. In this configuration, a maximum shear component is acting along the B/P TB. The initial configuration is shown in Fig. 7. The dimension of this simulation system is $20 \times 32 \times 20 \text{ nm}^3$, containing 523,568 atoms. The stain rate is 5.0 $\times\,10^{10}/\text{s}.$ Two crystals are bonded together and have a misorientation of 90° with a zone axis of [1210]. The basal planes of the left crystal (twin) are colored in red and blue and the basal planes of the right crystal (parent) are colored in white and yellow alternately to show the ...ABABAB... HCP stacking sequence in the two twin crystals. A tensile load was applied along the horizontal direction, which makes 45° with basal planes of both crystals, and nearly parallel to the $\{10\bar{1}2\}$ plane or perpendicular to the {1012} plane. Atoms inside the red box were selected for computing the energy barrier of the transformation from HCP to FCC.

Fig. 8 shows the evolution of the stress of the simulation box under the tensile loading. As the deformation proceeds, the stress increases. At ~ 80 ps, an FCC structure starts nucleating on the B/P TB. As the HCP transforms to the FCC, the stress continues to increase. At ~ 280 ps, dislocation slip is activated, causing the stress to decrease. The four red dots correspond to the snapshots displayed in Fig. 9 which shows the evolution of the FCC phase in time sequence.

Fig. 9a shows the relaxed structure of the initial TB at \sim 40 ps, which is a B/P type interface and makes 45° with the loading direction. No FCC phase is nucleated yet. Around \sim 125 ps, a four layer FCC structure is nucleated at the lower portion of the TB (Fig. 9b). The HCP and FCC structure are colored in red and green, respectively. As the strain further increases, the FCC structure grows layer by layer toward the parent. At 285 ps (Fig. 9c), the FCC phase has become rather thick. Compared to the FCC phase in compression (Fig. 5) and tension (Fig. 6), the thickness of the FCC with a high shear component is much larger. At this time, a $\{10\bar{1}1\}$ partial dislocation emerges, which corresponds to the decrease of stress in Fig. 8. At 800 ps (Fig. 9d), the FCC phase continues to thicken and the volume fraction of the FCC structure reaches up to \sim 14%. It can be seen that the transformation of HCP \rightarrow

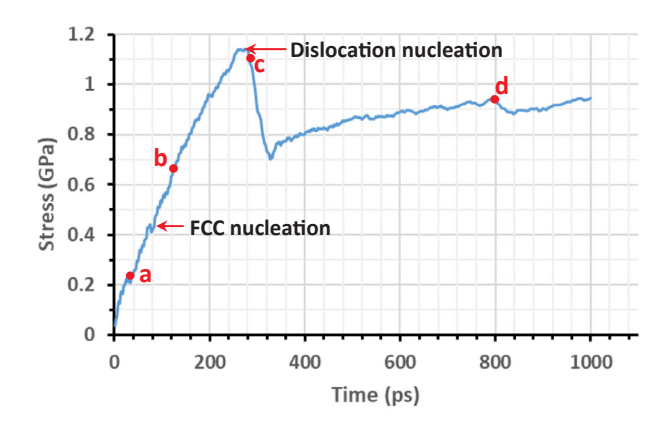


Fig. 8. Evolution of the tensile stress of the simulation system during deformation. The FCC phase nucleates at \sim 80 ps. As the HCP parent transforms to the FCC, the stress increases. After the dislocation nucleates at \sim 280 ps, the stress drops. The snapshots corresponding to the four red dots are displayed in Fig. 9.

FCC contributes the most to the overall plastic strain, because only a very limited number of dislocations are activated.

To better resolve the mechanism of the HCP \rightarrow FCC transformation, the boxed region in Fig. 9d was magnified and analyzed in Fig. 10. First, we applied the CNA to the system (Fig. 10a). The FCC and HCP phase can be well distinguished and identified. It can be readily seen that the OR is $(0002)_T \| (111)_{FCC} \| (10\bar{1}0)_P$. For comparison, Fig. 10b shows the analysis on the same region without CNA. It can be found that the FCC structure grows at the expense of the HCP parent lattice. Also, it is obvious that the shear in the phase transformation generates a tensile strain along the c-axis of the parent. The lattice transformation is achieved by $(10\bar{1}0)_P \rightarrow (111)_{FCC}$, consistent with the analysis in Figs. 5 and 6.

The energy evolution for the atoms contained in the selected box in Fig. 7 was computed and plotted in Fig. 11. The box contains 524 atoms. As the deformation continues, the energy gradually increases due to the elastic deformation. At 100 ps, a sharp increase in energy occurs, corresponding to the nucleation of the FCC structure at B/P TB. After the HCP structure of the selected box is completely transformed to the FCC, the energy drops. Thus, the energy barrier of the transformation from the HCP parent lattice to the FCC is $\sim 20 \, \text{meV/atom}$, which is close to the energy barrier calculated in Fig. 4a.

4. Analysis and discussion

4.1. Formation of FCC at B/P TB as related to non-classical twinning behavior

The results in Figs. 3-6 show that irrespective of tension or compression in the simulations, an FCC phase can be formed along the B/P TB. This phenomenon is another manifestation of the non-classical twinning behavior of $\{10\bar{1}2\}\langle10\bar{1}\bar{1}\rangle$ mode in HCP metals that cannot be accounted for by the classical theory or shear-dominated twinning theories. For twinning in FCC and BCC materials, TBs always coincide with the twinning plane as required by the invariant plane strain condition. For FCC, the twinning plane, i.e. the first invariant plane is the close-packed {111} and the twinning Burgers vector is $\frac{1}{6}\langle 1\bar{2}1\rangle$; for BCC, the twinning plane is {1 1 2} and the twinning Burgers vector is $\frac{1}{6}\langle 11\bar{1}\rangle$. In these high symmetry crystal structures, glide of well-defined twinning dislocation lines or loops on the TBs grows the twin in both the thickness and the lateral directions. For other twinning modes in HCP materials, i.e. $\{10\bar{1}1\}\langle10\bar{1}\bar{2}\rangle$, $\{11\bar{2}2\}\langle11\bar{2}\bar{3}\rangle$, $\{11\bar{2}1\}\langle11\bar{2}\bar{6}\rangle$ [10], TBs mostly coincide with the twinning planes, although details of the twinning dislocations (usually zonal dislocations) are still incomplete and more research is needed. Deviations between actual TBs and the

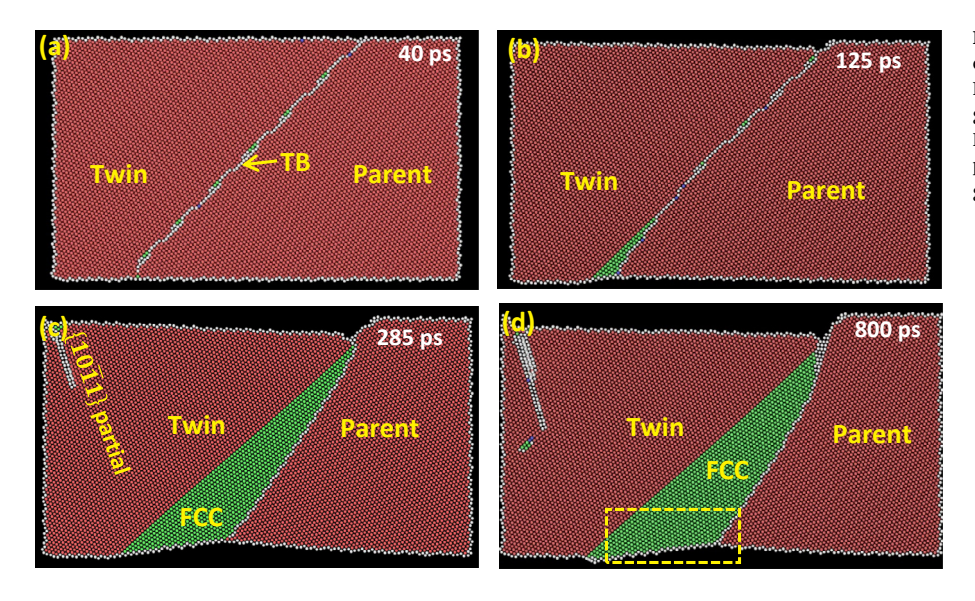


Fig. 9. Transformation from HCP to FCC in time sequence. (a) The relaxed twin boundary (TB). (b) An FCC phase is nucleated at the TB. (c) The FCC phase grows into the parent by transforming the parent HCP lattice (in red) into FCC (in green). (d) The FCC phase expands as the strain increases. The boxed region is analyzed in Fig. 10.

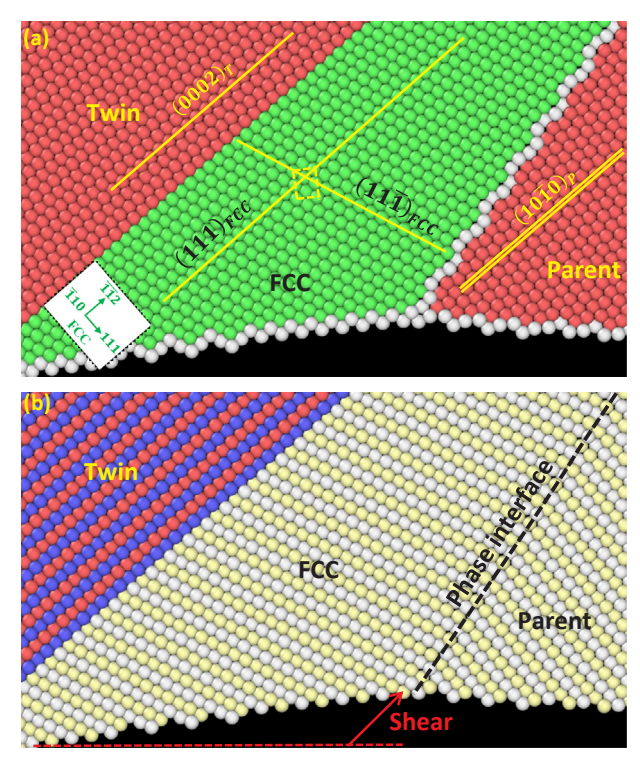


Fig. 10. Analysis of the boxed region in Fig. 9d. (a) Common neighbor analysis (CNA) of orientation relationship (OR) between the parent, FCC and twin. The OR satisfies $(0\ 0\ 0\ 2)_T \|(1\ 1\ 1)_{FCC}\|(1\ 0\ \bar{1}\ 0)_P$. (b) Without CNA, it can be seen that the FCC phase is transformed from the parent such that the $(1\ 1\ 1)_{FCC}$ plane is transformed from the $(1\ 0\ \bar{1}\ 0)_P$ of the parent. The red arrow denotes the shear on consecutive $(1\ 1\ 1)$ planes. Shear and shuffles are needed in this transformation.

twinning planes can sometimes be observed due to accommodation effects, twin-slip interactions and twin-twin interactions, but such deviations are usually small. On the atomic scale, the TBs still largely coincide with the twinning plane. These twinning modes can be well described inside the framework of the classical twinning theory: (1) a homogeneous simple shear can be definitively defined on the twinning plane which is the first invariant plane in the sense that the structure of the twinning plane remains undistorted. Because of this invariant plane strain (IPS) condition, the TB and the twinning plane must coincide; (2) the homogeneous simple shear is accomplished by twinning dislocations for FCC and BCC metals and by zonal twinning dislocations for

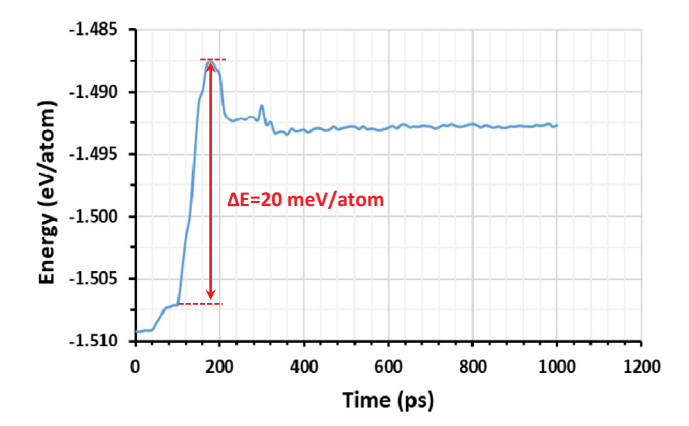


Fig. 11. Evolution of energy during transformation from HCP to FCC. The energy barrier for the phase transformation is about 20 meV/atom.

HCP metals [31,49]. In classical twinning behavior, it is unlikely for a new phase that has a different crystal structure from that of the twin crystals to be formed on the TB because the presence of such a phase transformation would disrupt the simple shear on the TB.

In stark contrast to other twinning modes mentioned above, $\{10\bar{1}2\}\langle10\bar{1}\bar{1}\}$ twinning mode completely departs from the classical twinning behavior. It has been extensively observed in experimental observations that actual {1012} TBs can be extremely incoherent [14,18]; no unique value of misorientation angle exists [18,23]; migrating TBs almost do not interact with precipitates but entirely engulf precipitates [32,50]; the Schmid law oftentimes is not followed [51,52]; twin-slip interaction almost has no contribution to work hardening [8,53]; when different twin variants impinge and interact, very abnormal interfaces can be formed [54]. The presence of an FCC phase on TBs further corroborates that this particular twinning mode completely deviates from classical twinning. That is, {10 1 2} twinning mode cannot be mediated by twinning dislocations or other types of defects related to shearing vectors, it can only be mediated by atomic shuffling. As shown in Figs. 3 and 6, when the TBs are migrating, the boundary plane does not align with any specifically defined crystallographic plane. It should be noted that this important feature is not only observed in our simulations, but also observed extensively by other researchers [55,56]. Despite that "disconnections" and "disclinations" have been defined for such incoherent TBs, as pointed out in recent works [20,55,56], the actual twinning mechanism in those reports of "disconnections" and "disclinations" is exactly the same as the Li-Ma shuffling model [24] in

which a parent basal plane is transformed to a twin prismatic plane, and a parent prismatic plane is transformed to a twin basal plane. This lattice transformation must distort the $\{1\,0\,\bar{1}\,2\}$ twinning plane and thus no twinning shear can occur on the twinning plane [14,23]. The breakdown of the invariant plane strain condition and the absence of a homogeneous simple shear render this twinning mode unique from other twinning modes. Therefore, the formation of an FCC phase at TBs is permissible because there is no twinning shear and no twinning dislocations at TBs which are very incoherent.

4.2. $HCP \rightarrow FCC$ transformation driven by misfit strain

It can be easily seen that, during compression perpendicular to the c-axis of the parent (Fig. 3) and tension along the c-axis of the parent (Fig. 6), the actual effect of the deformation processes is not a shearing which is typical in dislocation dominated plastic deformation but a stretching. In the case of compression (Fig. 3), the atoms of the basal planes of the parent become the atoms of the prismatic planes of the twin, and this can be seen from the white atoms on the surfaces of the twin crystals. As the atoms of the parent are being moved to the twin positions by shuffling, a misfit strain is produced between the parent and the twin. The misfit strain is manifested by the two bulges on the surfaces of the twin. In the meantime, a contraction is produced along the compression direction. Thus, two strain components are generated by the $\{10\bar{1}2\}\langle10\bar{1}\bar{1}\rangle$ twinning mode: an extension along the *c*-axis of the parent and a contraction perpendicular to the *c*-axis of the parent. In the case of tension (Fig. 6), a similar behavior can be seen. This important feature is totally different from shear-dominated twinning modes in FCC, BCC and HCP metals in which the overall strain produced by twinning is generated by the shear displacement component along the Burgers vector of the twinning dislocations which must lie in the twinning plane.

It can be calculated [22] that, when the parent crystal is reoriented by 90° around the $\langle 1\,\bar{2}\,1\,0\rangle$ zone axis during $\{1\,0\,\bar{1}\,2\}$ twinning, a global strain would be generated, this strain is calculated as $\varepsilon=\frac{\sqrt{3}-\lambda}{\lambda}$ for extension along the c-axis, and $\varepsilon=\frac{\lambda-\sqrt{3}}{\sqrt{3}}$ for the contraction perpendicular to the c-axis (λ is the c/a ratio, ~ 1.624 for Mg). The HCP \rightarrow FCC transformation on the TB can effectively accommodate the misfit strain between the parent and the twin. Without the FCC phase, the misfit strain will cause large lattice distortion in the regions close to the free surfaces (Fig. 3b and c). When the FCC phase is formed, the distorted lattice is replaced by the non-distorted FCC lattice (Fig. 3d). However, the consequence of this phase transformation is that the FCC phase hinders the TB migration, and thus a higher stress is needed for twin growth. If the misorientation angle slightly deviates from 90°, say 86.3° which is the theoretical value of the misorientation angle, these two strain components still exist, but vary only by a few percent.

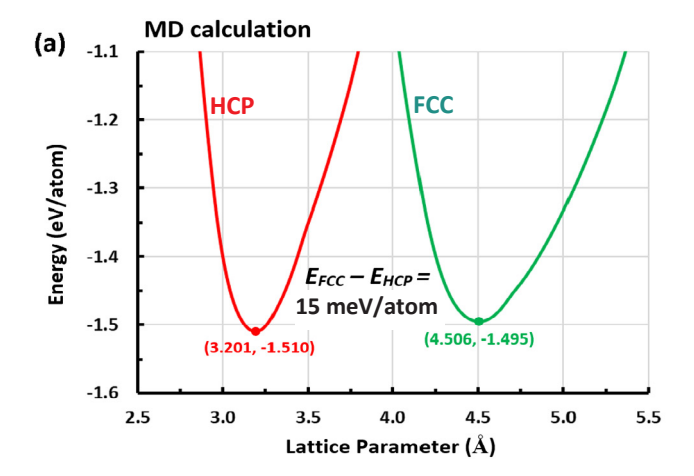
As shown in Figs. 5, 6 and 10, the transformation from HCP to FCC is accomplished by the transformation of a double-layered prismatic plane in HCP to a closed packed (111)_{FCC} plane. It is noted that basal stacking faults created by Shockley partial dislocations can also produce an FCC structure, but this is not the case in our simulations. As analyzed in Fig. 5, the amount of the shear displacement along the [0002] direction of HCP parent is ~0.10 nm on every green close-packed plane of FCC. This magnitude is about half of the Burgers vector of a Shockley partial. Also, formation of an FCC by basal stacking faults does not involve atomic shuffles. However, the double-layered prismatic plane cannot be transformed to a single layered $(111)_{FCC}$ plane solely by shear. Thus, atomic shuffling must be involved to carry the atoms to the correct positions in FCC. The displacement caused by shuffling is $\sim \frac{\sqrt{3}}{6}a$, which is equal to the spacing between the double layers of a $\{10\bar{1}0\}$ prismatic plane. Also, there must be lattice distortion that needs to be adjusted so that a correct interplanar spacing of the $(11\bar{1})_{FCC}$ planes is reached. Hence, the FCC structure can be transformed from HCP by two simultaneous processes, i.e. shear and shuffle. It is also

worth noting that the transformation from HCP to FCC at the TB is reversible. As shown in Fig. 3e-3 g, when the migration of TB restarts, the FCC structure transforms to the HCP twin. As shown in Fig. 4a, the energy barrier for the transformation from FCC to HCP is pretty low ($\sim 8.5 \, \text{meV/atom}$), which is less than half of that for transformation from HCP to FCC and even lower than the energy barrier for twin growth. From the simulations (Fig. 3), the reverse transformation only involves atomic shuffles and this is likely the reason why the energy barrier for the reverse transformation is very low.

In simulation of deformation twinning of Ti, it was reported that an FCC phase can form at a twin boundary due to the gliding of basal partial dislocation [26], and the basal partial dislocation was characterized with a double-layered structure [25,57]. In our work, the FCC structure is transformed from the parent and grows layer by layer (Fig. 3b–d), indicating that the FCC structure is not generated by Shockley partials on the basal plane of the twin. Thus, the mechanism of the transformation observed in our simulation is different.

There have been reports of phase transformations activated during plastic deformation in which strain localization occurs. The phase transformations can serve as additional deformation modes to accommodate local strain and prevent material failure [58]. In deformation of biomedical Co–Cr–Mo alloy [59], transformation of γ -FCC phase to ϵ -HCP phase was observed near the annealing twin boundaries, which was attributed to the incompatibility of plastic strain across the TBs. Recently, Wang et al. [60] reported a deformation induced structural transition in body-centered cubic molybdenum, which is caused by the local strain concentration. It was also found that this type of phase transformation only occurs when the conventional deformation mechanisms, e.g., twinning, dislocation slip and grain boundary sliding, are suppressed. However, it should be noted that the transformation from HCP to FCC at B/P interfaces has not been reported in Mg and Mg alloys in experimental observations.

To exclude the possibility that the HCP \rightarrow FCC transformation on the B/P TB was driven by the energy difference between the FCC and HCP, we calculated the lattice energy of the two phases with MD and DFT. Ideally, free energies of the two phases should be calculated and a method was provided by Freitas et al. [61]. This method has been applied in calculating the free energies of interfaces and crystalline structures [62,63]. For pure Mg, it is well known that the equilibrium phase at ambient pressure and temperature is HCP and FCC Mg is nonequilibrium. Fig. 12 shows the calculated energies of HCP and FCC Mg as a function of lattice parameter. In Fig. 12a, the EAM potential [30] was used for MD calculation. It can be observed that the HCP has a lower energy ($-1.510 \, \text{eV/atom}$) than the FCC ($-1.495 \, \text{eV/atom}$) at the lattice parameter corresponding to the energy minimum. Thus, the energy of HCP is 15 meV/atom lower than that of the FCC. As a comparison, the results from DFT calculation were plotted in Fig. 12b. It can be seen that the energy difference between HCP and FCC is 12 meV/ atom, which is very close to the MD result. These calculated energies are consistent with the values reported by Althoff et al. [64] who showed that the energy of HCP is 11 meV/atom lower than that of FCC. These calculations indicate that the $HCP \rightarrow FCC \rightarrow HCP$ phase transformations are driven by the misfit strain energy. We expect that such a phase transformation can be observed by using in-situ TEM observation of deformation twinning in a single crystal. Without a doubt, further study is needed to validate the simulation results. One of the interesting features revealed in the simulations is that formation of an FCC phase at B/P interfaces impedes the TB migration and a higher stress is needed for continued migration. It has been shown that, {1012} extension twinning dominates the low stress stage deformation in textured Mg and Mg alloys [9,11]. Thus, if the FCC phase can be promoted at B/P interfaces during deformation, the strength of Mg alloys can be improved. Additionally, due to the superior ductility of FCC structures, the mechanical properties of Mg and other HCP metals could possibly be improved.



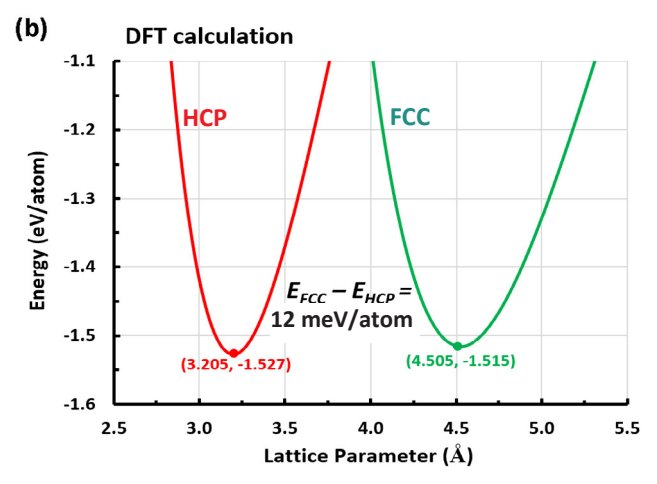


Fig. 12. The energy of HCP and FCC Mg as a function of lattice parameter. (a) Atomistic calculation by using the EAM potential. (b) DFT calculation.

5. Conclusions

HCP \rightarrow FCC \rightarrow HCP phase transformations were observed at $\{1\,0\,\bar{1}\,2\}$ TBs in the atomistic simulations of TB migration in pure Mg. The following conclusions can be reached.

- The transformation of FCC structure is a result of local misfit strain produced by the lattice transformation from the parent to the twin. The misfit strain between the parent and the twin generates lattice distortion in the region near the B/P TB. As a result, HCP → FCC transformation occurs to compensate the lattice distortion. The HCP → FCC transformation impedes TB migration.
- 2. The HCP \rightarrow FCC transformation is accomplished by a combination of shear and shuffle, transforming a double-layered prismatic plane of the parent to a single-layered (111) plane of the FCC phase. The corresponding orientation relationship is a new type, i.e., $(111)_{FCC}$ || $\{10\bar{1}0\}_{HCP}$.
- 3. The FCC phase at the B/P TB transforms to the HCP twin as the strain increases, and this reverse transformation may only involve atomic shuffles.
- 4. The energy barrier of the transformation from HCP parent lattice to FCC structure is ~ 21 meV/atom, while the energy barrier for twin growth is about ~ 11.9 meV/atom. The energy barrier for the reverse transformation from FCC to HCP twin is ~ 8.5 meV/atom.

CRediT authorship contribution statement

Peng Chen: Investigation, Writing - original draft. **Fangxi Wang:** Validation. **Bin Li:** Writing - review & editing, Supervision.

Acknowledgement

Bin Li gratefully thanks support from the U.S. National Science Foundation (NSF) (CMMI-1635088).

References

- A. Akhtar, Basal slip and twinning in α-titanium single crystals, Metall. Trans. A 6 (1975) 1105, https://doi.org/10.1007/BF02661366.
- [2] J.A. Yasi, T. Nogaret, D.R. Trinkle, Y. Qi, L.G.H. Jr, W.A. Curtin, Basal and prism dislocation cores in magnesium: comparison of first-principles and embedded-atompotential methods predictions, Model. Simul. Mater. Sci. Eng. 17 (2009) 055012, https://doi.org/10.1088/0965-0393/17/5/055012.
- [3] M. Liao, B. Li, M.F. Horstemeyer, Interaction between prismatic slip and a Mg17Al12 precipitate in magnesium, Comput. Mater. Sci. 79 (2013) 534–539, https://doi.org/10.1016/j.commatsci.2013.07.016.
- [4] B. Li, E. Ma, Pyramidal slip in magnesium: dislocations and stacking fault on the 1011 plane, Philos. Mag. 89 (2009) 1223–1235, https://doi.org/10.1080/ 14786430902936707.
- [5] H. Fan, J.A. El-Awady, Towards resolving the anonymity of pyramidal slip in magnesium, Mater. Sci. Eng. A 644 (2015) 318–324, https://doi.org/10.1016/j. msea.2015.07.080.
- [6] H. Fan, J. Tang, X. Tian, Q. Wang, X. Tian, J.A. El-Awady, Core structures and mobility of ⟨c⟩ dislocations in magnesium, Scr. Mater. 135 (2017) 37–40, https:// doi.org/10.1016/j.scriptamat.2017.03.012.
- [7] Y. Tang, J.A. El-Awady, Formation and slip of pyramidal dislocations in hexagonal close-packed magnesium single crystals, Acta Mater. 71 (2014) 319–332, https:// doi.org/10.1016/j.actamat.2014.03.022.
- [8] P. Chen, F. Wang, B. Li, Dislocation absorption and transmutation at 10–12 twin boundaries in deformation of magnesium, Acta Mater. 164 (2019) 440–453, https://doi.org/10.1016/j.actamat.2018.10.064.
- [9] E. Kelley, W. Hosford, Plane-strain compression of magnesium and magnesium alloy crystals, Trans. Met. Soc. AIME 242 (1968) 5–13.
- [10] J.W. Christian, S. Mahajan, Deformation twinning, Prog. Mater. Sci. 39 (1995) 1–157.
- [11] P. Chen, B. Li, D. Culbertson, Y. Jiang, Contribution of extension twinning to plastic strain at low stress stage deformation of a Mg-3Al-1Zn alloy, Mater. Sci. Eng. A 709 (2018) 40–45, https://doi.org/10.1016/j.msea.2017.10.038.
- [12] Z.S. Basinski, M.S. Szczerba, M. Niewczas, J.D. Embury, S.J. Basinski, The transformation of slip dislocations during twinning of copper-aluminum alloy crystals, Rev. Métall. 94 (1997) 1037–1044, https://doi.org/10.1051/metal/199794091037
- [13] X. Li, Y. Wei, L. Lu, K. Lu, H. Gao, Dislocation nucleation governed softening and maximum strength in nano-twinned metals, Nature 464 (2010) 877–880, https://doi.org/10.1038/nature08929.
- [14] B. Li, X.Y. Zhang, Twinning with zero twinning shear, Scr. Mater. 125 (2016) 73–79, https://doi.org/10.1016/j.scriptamat.2016.07.004.
- [15] S.G. Song, G.T. Gray, Structural interpretation of the nucleation and growth of deformation twins in Zr and Ti—II. Tem study of twin morphology and defect reactions during twinning, Acta Metall. Mater. 43 (1995) 2339–2350, https://doi. org/10.1016/0956-7151(94)00434-X.
- [16] S.G. Song, G.T. Gray, Structural interpretation of the nucleation and growth of deformation twins in Zr and Ti—I. Application of the coincidence site lattice (CSL) theory to twinning problems in h.c.p. structures, Acta Metall. Mater. 43 (1995) 2325–2337, https://doi.org/10.1016/0956-7151(94)00433-1.
- [17] C. Cayron, R. Logé, Evidence of new twinning modes in magnesium questioning the shear paradigm, J. Appl. Crystallogr. 51 (2018) 809–817, https://doi.org/10.1107/ S1600576718005678.
- [18] X.Y. Zhang, B. Li, X.L. Wu, Y.T. Zhu, Q. Ma, Q. Liu, P.T. Wang, M.F. Horstemeyer, Twin boundaries showing very large deviations from the twinning plane, Scr. Mater. 67 (2012) 862–865, https://doi.org/10.1016/j.scriptamat.2012.08.012.
- [19] P.G. Partridge, E. Roberts, The formation and behaviour of incoherent twin boundaries in hexagonal metals, Acta Metall. 12 (1964) 1205–1210, https://doi. org/10.1016/0001-6160(64)90103-8.
- [20] A. Serra, D.J. Bacon, A new model for 10-12 twin growth in hcp metals, Philos. Mag. A. 73 (1996) 333-343, https://doi.org/10.1080/01418619608244386.
- [21] A. Serra, D.J. Bacon, R.C. Pond, The crystallography and core structure of twinning dislocations in H.C.P. metals, Acta Metall. 36 (1988) 3183–3203, https://doi.org/ 10.1016/0001-6160(88)90054-5.
- [22] B. Li, X.Y. Zhang, Global strain generated by shuffling-dominated {101-2} < 10-1-1 > twinning, Scr. Mater. 71 (2014) 45–48, https://doi.org/10.1016/j.scriptamat.
- [23] X.Y. Zhang, B. Li, Q. Sun, On the 10–12 "twinning shear" measured from line deflection, Scr. Mater. 159 (2019) 133–136, https://doi.org/10.1016/j.scriptamat. 2018.09.027.
- [24] B. Li, E. Ma, Atomic shuffling dominated mechanism for deformation twinning in magnesium, Phys. Rev. Lett. 103 (2009) 035503, https://doi.org/10.1103/

- PhysRevLett. 103.035503.
- [25] X.Y. Zhang, B. Li, Q. Liu, Non-equilibrium basal stacking faults in hexagonal close-packed metals, Acta Mater. 90 (2015) 140–150, https://doi.org/10.1016/j.actamat. 2015.02.036.
- [26] J. Ren, Q. Sun, L. Xiao, X. Ding, J. Sun, Phase transformation behavior in titanium single-crystal nanopillars under [0001] orientation tension: a molecular dynamics simulation, Comput. Mater. Sci. 92 (2014) 8–12, https://doi.org/10.1016/j. commatsci.2014.05.018.
- [27] J.P. Hirth, J. Wang, C.N. Tomé, Disconnections and other defects associated with twin interfaces, Prog. Mater. Sci. 83 (2016) 417–471, https://doi.org/10.1016/j. pmatsci.2016.07.003.
- [28] M.S. Daw, M.I. Baskes, Semiempirical, quantum mechanical calculation of hydrogen embrittlement in metals, Phys. Rev. Lett. 50 (1983) 1285–1288, https://doi. org/10.1103/PhysRevLett. 50.1285.
- [29] M.S. Daw, M.I. Baskes, Embedded-atom method: derivation and application to impurities, surfaces, and other defects in metals, Phys. Rev. B 29 (1984) 6443–6453, https://doi.org/10.1103/PhysRevB.29.6443.
- [30] X.-Y. Liu, J.B. Adams, F. Ercolessi, J.A. Moriarty, EAM potential for magnesium from quantum mechanical forces, Model. Simul. Mater. Sci. Eng. 4 (1996) 293, https://doi.org/10.1088/0965-0393/4/3/004.
- [31] B. Li, E. Ma, Zonal dislocations mediating {101-1}<10-1-2> twinning in magnesium, Acta Mater. 57 (2009) 1734–1743, https://doi.org/10.1016/j.actamat.2008.12.
- [32] F.X. Wang, B. Li, Origin of deflection of precipitates during interaction with a migrating twin boundary in magnesium alloys, Comput. Mater. Sci. 154 (2018) 472–480, https://doi.org/10.1016/j.commatsci.2018.08.020.
- [33] A. Stukowski, Visualization and analysis of atomistic simulation data with OVITO-the Open Visualization Tool, Model. Simul. Mater. Sci. Eng. 18 (2010) 015012, https://doi.org/10.1088/0965-0393/18/1/015012.
- [34] J.D. Honeycutt, H.C. Andersen, Molecular dynamics study of melting and freezing of small Lennard-Jones clusters, J. Phys. Chem. 91 (1987) 4950–4963, https://doi. org/10.1021/j100303a014.
- [35] G. Kresse, J. Hafner, Ab initio molecular dynamics for liquid metals, Phys. Rev. B 47 (1993) 558–561, https://doi.org/10.1103/PhysRevB.47.558.
- [36] G. Kresse, J. Furthmüller, Efficiency of ab-initio total energy calculations for metals and semiconductors using a plane-wave basis set, Comput. Mater. Sci. 6 (1996) 15–50, https://doi.org/10.1016/0927-0256(96)00008-0.
- [37] G. Kresse, J. Furthmüller, Efficient iterative schemes for ab initio total-energy calculations using a plane-wave basis set, Phys. Rev. B 54 (1996) 11169–11186, https://doi.org/10.1103/PhysRevB.54.11169.
- [38] P.E. Blöchl, Projector augmented-wave method, Phys. Rev. B 50 (1994) 17953–17979, https://doi.org/10.1103/PhysRevB.50.17953.
- [39] G. Kresse, D. Joubert, From ultrasoft pseudopotentials to the projector augmentedwave method, Phys. Rev. B 59 (1999) 1758–1775, https://doi.org/10.1103/ PhysRevB.59.1758.
- [40] J.P. Perdew, K. Burke, M. Ernzerhof, Generalized gradient approximation made simple, Phys. Rev. Lett. 77 (1996) 3865–3868, https://doi.org/10.1103/ PhysRevLett. 77 3865
- [41] J. Wang, S.K. Yadav, J.P. Hirth, C.N. Tomé, I.J. Beyerlein, Pure-shuffle nucleation of deformation twins in hexagonal-close-packed metals, Mater. Res. Lett. 1 (2013) 126–132, https://doi.org/10.1080/21663831.2013.792019.
- [42] Q. Yu, J. Kacher, C. Gammer, R. Traylor, A. Samanta, Z. Yang, A.M. Minor, In situ TEM observation of FCC Ti formation at elevated temperatures, Scr. Mater. 140 (2017) 9–12, https://doi.org/10.1016/j.scriptamat.2017.06.033.
- [43] H. Zhao, X. Hu, M. Song, S. Ni, Mechanisms for deformation induced hexagonal close-packed structure to face-centered cubic structure transformation in zirconium, Scr. Mater. 132 (2017) 63–67, https://doi.org/10.1016/j.scriptamat.2017.01.034.
- [44] H. Zhao, M. Song, S. Ni, S. Shao, J. Wang, X. Liao, Atomic-scale understanding of stress-induced phase transformation in cold-rolled Hf, Acta Mater. 131 (2017) 271–279, https://doi.org/10.1016/j.actamat.2017.03.058.
- [45] D.H. Hong, T.W. Lee, S.H. Lim, W.Y. Kim, S.K. Hwang, Stress-induced hexagonal close-packed to face-centered cubic phase transformation in commercial-purity

- titanium under cryogenic plane-strain compression, Scr. Mater. 69 (2013) 405–408, https://doi.org/10.1016/j.scriptamat.2013.05.038.
- [46] X. Hu, H. Zhao, S. Ni, M. Song, Grain refinement and phase transition of commercial pure zirconium processed by cold rolling, Mater. Charact. 129 (2017) 149–155, https://doi.org/10.1016/j.matchar.2017.04.037.
- [47] M. An, Q. Deng, Y. Li, H. Song, M. Su, J. Cai, Molecular dynamics study of tension-compression asymmetry of nanocrystal α-Ti with stacking fault, Mater. Des. 127 (2017) 204–214, https://doi.org/10.1016/j.matdes.2017.04.076.
- [48] H.C. Wu, A. Kumar, J. Wang, X.F. Bi, C.N. Tomé, Z. Zhang, S.X. Mao, Rolling-induced face centered cubic titanium in hexagonal close packed titanium at room temperature, Sci. Rep. 6 (2016) srep24370, https://doi.org/10.1038/srep24370.
- [49] B. Li, H.E. Kadiri, M.F. Horstemeyer, Extended zonal dislocations mediating twinning in titanium, Philos. Mag. 92 (2012) 1006–1022, https://doi.org/10.1080/14786425 2011 637085
- [50] M.A. Gharghouri, G.C. Weatherly, J.D. Embury, The interaction of twins and precipitates in a Mg-7.7 at.% Al alloy, Philos. Mag. A. 78 (1998) 1137–1149, https://doi.org/10.1080/01418619808239980.
- [51] M.Z. Bian, K.S. Shin, 10–12 twinning behavior in magnesium single crystal, Met. Mater. Int. 19 (2013) 999–1004, https://doi.org/10.1007/s12540-013-5012-4.
- [52] Z. McClelland, B. Li, S.J. Horstemeyer, S. Brauer, A.A. Adedoyin, L.G. Hector, M.F. Horstemeyer, Geometrically necessary twins in bending of a magnesium alloy, Mater. Sci. Eng. A. 645 (2015) 298–305, https://doi.org/10.1016/j.msea.2015.08.
- [53] P. Chen, B. Li, D. Culbertson, Y. Jiang, Negligible effect of twin-slip interaction on hardening in deformation of a Mg-3Al-1Zn alloy, Mater. Sci. Eng. A 729 (2018) 285–293, https://doi.org/10.1016/j.msea.2018.05.067.
- [54] P. Chen, F. Wang, J. Ombogo, B. Li, Formation of 60° (01-10) boundaries between 10–12 twin variants in deformation of a magnesium alloy, Mater. Sci. Eng. A 739 (2019) 173–185, https://doi.org/10.1016/j.msea.2018.10.029.
- [55] C.D. Barrett, H. El Kadiri, The roles of grain boundary dislocations and disclinations in the nucleation of 10–12 twinning, Acta Mater. 63 (2014) 1–15, https://doi.org/ 10.1016/j.actamat.2013.09.012.
- [56] H.A. Khater, A. Serra, R.C. Pond, Atomic shearing and shuffling accompanying the motion of twinning disconnections in Zirconium, Philos. Mag. 93 (2013) 1279–1298, https://doi.org/10.1080/14786435.2013.769071.
- [57] B. Li, Q.W. Zhang, S.N. Mathaudhu, Basal-pyramidal dislocation lock in deformed magnesium, Scr. Mater. 134 (2017) 37–41, https://doi.org/10.1016/j.scriptamat. 2017.02.040.
- [58] D.A. Porter, K.E. Easterling, M. Sherif, Phase Transformations in Metals and Alloys, (Revised Reprint). CRC Press. 2009.
- [59] Y. Koizumi, S. Suzuki, K. Yamanaka, B.-S. Lee, K. Sato, Y. Li, S. Kurosu, H. Matsumoto, A. Chiba, Strain-induced martensitic transformation near twin boundaries in a biomedical Co–Cr–Mo alloy with negative stacking fault energy, Acta Mater. 61 (2013) 1648–1661, https://doi.org/10.1016/j.actamat.2012.11. 041.
- [60] S.J. Wang, H. Wang, K. Du, W. Zhang, M.L. Sui, S.X. Mao, Deformation-induced structural transition in body-centred cubic molybdenum, Nat. Commun. 5 (2014) 3433. https://doi.org/10.1038/ncomms4433.
- [61] R. Freitas, M. Asta, M. de Koning, Nonequilibrium free-energy calculation of solids using LAMMPS, Comput. Mater. Sci. 112 (2016) 333–341, https://doi.org/10. 1016/j.commatsci.2015.10.050.
- [62] R. Freitas, T. Frolov, M. Asta, Step free energies at faceted solid surfaces: theory and atomistic calculations for steps on the Cu(111) surface, Phys. Rev. B 95 (2017) 155444, https://doi.org/10.1103/PhysRevB.95.155444.
- [63] R. Freitas, R.E. Rudd, M. Asta, T. Frolov, Free energy of grain boundary phases: Atomistic calculations for Σ5(310)[001] grain boundary in Cu, Phys. Rev. Mater. 2 (2018) 093603, https://doi.org/10.1103/PhysRevMaterials. 2.093603.
- [64] J.D. Althoff, P.B. Allen, R.M. Wentzcovitch, J.A. Moriarty, Phase diagram and thermodynamic properties of solid magnesium in the quasiharmonic approximation, Phys. Rev. B 48 (1993) 13253–13260, https://doi.org/10.1103/PhysRevB.48. 13253.